nature photonics

LETTERS

PUBLISHED ONLINE: 4 APRIL 2011 | DOI: 10.1038/NPHOTON.2011.33

Nanofocusing of mid-infrared energy with tapered transmission lines

M. Schnell[1], P. Alonso-González[1], L. Arzubiaga[1], F. Casanova[1,2], L. E. Hueso[1,2], A. Chuvilin[1,2] and R. Hillenbrand[1,2]*

Mid-infrared radiation allows the analysis of a wide range of different material properties, including chemical composition and the structure of matter[1,2]. Infrared spectroscopy is therefore an essential analytical tool in many sciences and technologies. The diffraction limit, however, challenges the study of individual molecules and nanostructures, as well as the development of highly integrated mid-infrared optical devices[3]. Here, we experimentally demonstrate mid-infrared nanofocusing by propagating a mid-infrared surface wave along a tapered two-wire transmission line. The tapering results in a compression of the electromagnetic energy carried by the surface wave. By using infrared vector near-field microscopy[4,5], we directly visualize the evolution of the energy compression into a nanoscale confined infrared spot with a diameter of 60 nm (λ/150) at the taper apex. Our work opens the way to the development of chemical and biological sensing tools based on infrared surface waves, including miniaturized spectrometers and lab-on-a-chip integrated (bio)sensors.

An efficient route to circumventing the diffraction limit of conventional optical elements is based on the use of plasmonic antennas and waveguides[6–10]. These elements allow for the focusing, guiding and controlling of light on the nanometre scale and have therefore opened the door to optical imaging with nanoscale resolution[7], single-molecule Raman spectroscopy[11] and the development of metamaterials[12] and compact optical circuits[13].

The most common types of plasmonic antennas used for nanofocusing light are metal nanoparticles and nanorods. Tuned to be in resonance with the illuminating light wave, they convert propagating free-space radiation into highly concentrated near fields (also called hot spots or nanofoci) at the rod extremities or in nanoscale gaps between them[4,6–8,10,11,14]. Alternatively, nanofocusing of light can be achieved by the compression of surface plasmon polaritons (SPPs) propagating along tapered metal nanowires[15–20] or slot waveguides[21–23]. In contrast to antenna focusing, a propagating surface wave (rather than a free-space propagating wave) is focused. Applied in near-field microscopy[24] and tip-enhanced Raman spectroscopy[19], this mechanism offers an improved signal-to-background ratio, because the SPP excitation and the nanofocus at the taper apex are spatially separated. Waveguide focusing will also be an essential building block in future integrated plasmonic circuits[13], where SPPs are the carriers of optical energy.

For the development of nanoscale-resolving infrared and terahertz probes and ultrasensitive miniaturized spectrometers, however, one faces the problem that the surface waves are weakly guided in this spectral range[25]. An improved guiding of SPPs can be achieved by patterning metal surfaces, supporting surfaces waves called spoof SPPs[26]. For terahertz frequencies, it has been shown that spoof SPPs can be focused on corrugated tapered metal wires[27], but nanoscale dimensions are difficult to achieve. A different route with which to focus radiation is based on slot waveguides[28,29] where the electromagnetic energy is bound between two metal surfaces. A similar concept has recently been demonstrated experimentally[30], achieving a subwavelength focus of ~10 μm.

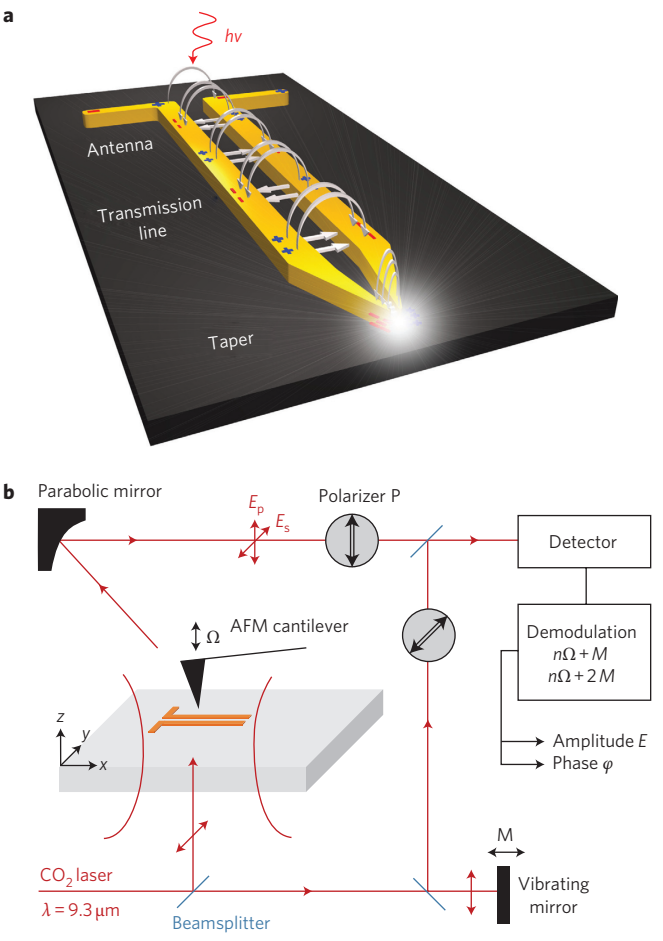

Figure 1 | Infrared nanofocusing with a tapered transmission line. **a**, Experimental concept. **b**, Transmission-mode near-field microscopy set-up[4]. The sample is illuminated from below with a weakly focused laser beam with polarization parallel to the dipole antenna. The near fields at the sample surface are scattered locally with the silicon tip of an atomic force microscope (AFM) and detected interferometrically, yielding amplitude and phase images of the near-field distribution by scanning the sample.

[1]CIC nanoGUNE Consolider, 20018 Donostia – San Sebastian, Spain, [2]IKERBASQUE, Basque Foundation for Science, 48011 Bilbao, Spain.
*e-mail: r.hillenbrand@nanogune.eu

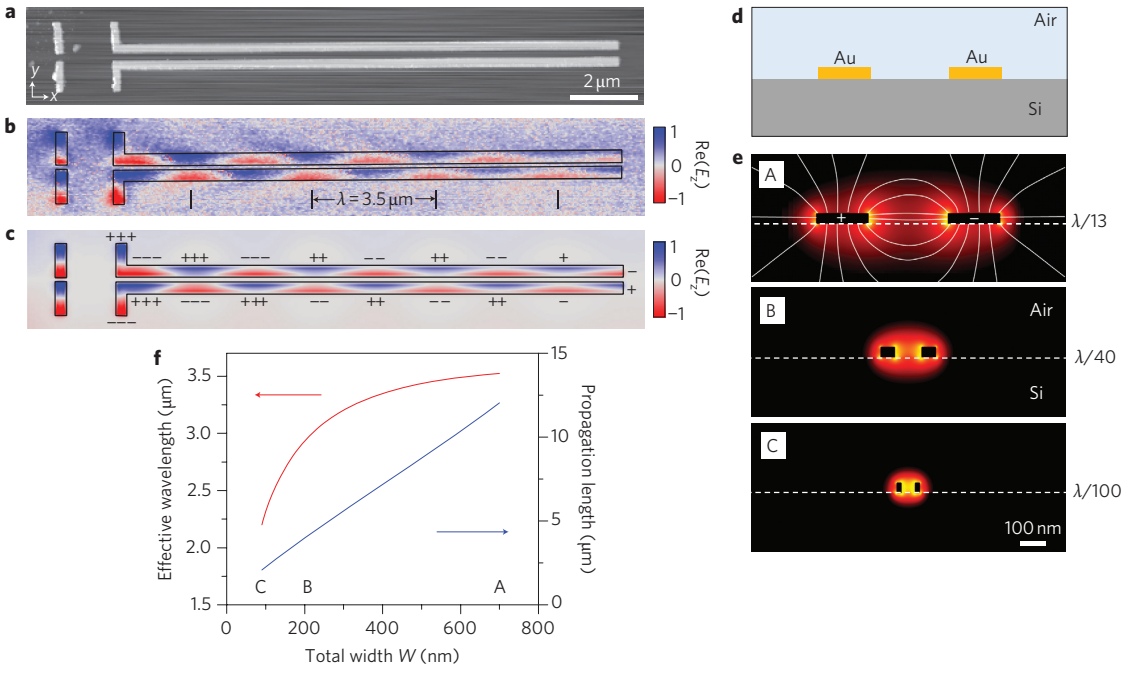

Figure 2 | Energy transport and propagation properties in two-wire transmission lines. a, Topography image of an antenna-coupled two-wire transmission line. Its calculated mode profile is shown in **e** (case A). **b**, Experimental near-field image taken at $\lambda = 9.3$ μm, showing $\mathrm{Re}(E_z) = |E_z|\cos(\varphi_z)$. **c**, Numerically calculated near-field image showing $\mathrm{Re}(E_z) = |E_z|\cos(\varphi_z)$. **d**, Schematics showing the cross-section of the two-wire transmission line, consisting of two 40-nm-thick parallel gold wires of width w, separated by a nanoscale gap of width g. **e**, Numerically calculated mode profiles (logarithmic scale) for transmission lines with (A) $w = 200$ nm and $g = 300$ nm, (B) $w = 56$ nm and $g = 100$ nm, and (C) $w = 20$ nm and $g = 50$ nm. **f**, Wavelength λ_{eff} and propagation length L as a function of the total transmission-line width $W = 2w + g$ while the wire width w and gap width g decrease simultaneously from $w = 200$ nm to 20 nm and $g = 300$ nm to 50 nm.

In the mid-infrared spectral range (in the transition between strong plasmonic and nearly ideal metallic behaviour), surface wave guiding is a widely unexplored terrain from both fundamental and applied perspectives. Recently, it has been demonstrated that mid-infrared energy can be guided with two-wire transmission lines, supporting propagating electromagnetic surface waves[31,32]. This concept is adapted from radiofrequency (RF) technology, with two-wire transmission lines having been used in the past to carry RF signals in television and radio applications.

Here, we predict and experimentally verify mid-infrared nanofocusing with tapered transmission lines by using compression of mid-infrared surface waves, as illustrated in Fig. 1a. We propose and realize a novel design including tapering of both the gap and the metal wires. Such an architecture is essential for providing a nanofocus at a sharply pointed extremity that can be used as a scanning probe tip or local sensing device. To verify experimentally the extraordinarily strong lateral confinement of the surface wave, we applied polarization- and phase-resolved scattering-type near-field optical microscopy (s-SNOM)[4,9], which we have recently developed to measure the vectorial field distribution of nanoscale optical fields (Fig. 1b; see Methods).

In this work, the transmission line consists of two parallel metal wires. A dipole antenna is attached to the non-tapered end of the two-wire transmission line. Infrared illumination with polarization parallel to the antenna can therefore launch a surface wave on the transmission line. This coupling mechanism is well known from RF technology and has been studied theoretically in the optical regime[33]. The launching of a surface wave and its propagation along mid-infrared transmission lines have been demonstrated recently[32]. In Fig. 2a–c, we first verified and characterized mid-infrared energy transport in untapered two-wire transmission lines to serve as a reference for the following nanofocusing experiments. To that end, the transmission line was imaged with our s-SNOM at a wavelength of $\lambda = 9.3$ μm. To visualize the field distribution and mode structure of the surface wave, we show in Fig. 2b the real part of the vertical near-field component, $\mathrm{Re}(E_z) = |E_z|\cos(\varphi_z)$, where $|E_z|$ is the near-field amplitude and φ_z the phase. We observe two dipolar-like modes on the antenna segments, with strong fields at the antenna ends and at the gap, as expected for a mid-infrared gap antenna[9]. The fields extend along the two wires, periodically changing their polarity. This provides direct experimental evidence of a propagating surface wave. We find a decreasing field strength with increasing distance x from the antenna (source), indicating propagation losses. From the oscillation period and the field decay we determine an effective wavelength $\lambda_{\mathrm{eff}} = 3.5$ μm and a propagation length $L \approx 8$ μm (defined as the $1/e$ decay of the field amplitude). The experimental image is in excellent qualitative agreement with numerical simulations of the near-field distribution (Fig. 2c) when we assume a refractive index of $n_{\mathrm{Si}} = 3.07$ for the silicon substrate. Our results show that mid-infrared energy can indeed be transported in our transmission lines of subwavelength-scale width $W = \lambda/13$.

Basic insights about the field confinement and propagation of mid-infrared energy ($\lambda = 9.3$ μm) in two-wire transmission lines were obtained by a numerical study using a finite-element mode solver (Fig. 2d–f). We considered infinitely long transmission lines of total width $W = 2w + g$, consisting of two parallel gold wires (width, w; height, 40 nm) on a silicon substrate, separated by an isolating gap of width g (Fig. 2d). In Fig. 2e, the antisymmetric mode solutions (cross-section of the near-field distribution) for three different transmission lines (A–C) are shown. We find that the near fields associated with these modes are strongly confined on the scale of the transmission-line width W, even for the extremely narrow transmission line C with $W = 90$ nm ($\lambda/100$). We analysed the propagation properties of the modes in Fig. 2f, showing the effective wavelength λ_{eff} and propagation length L when both the

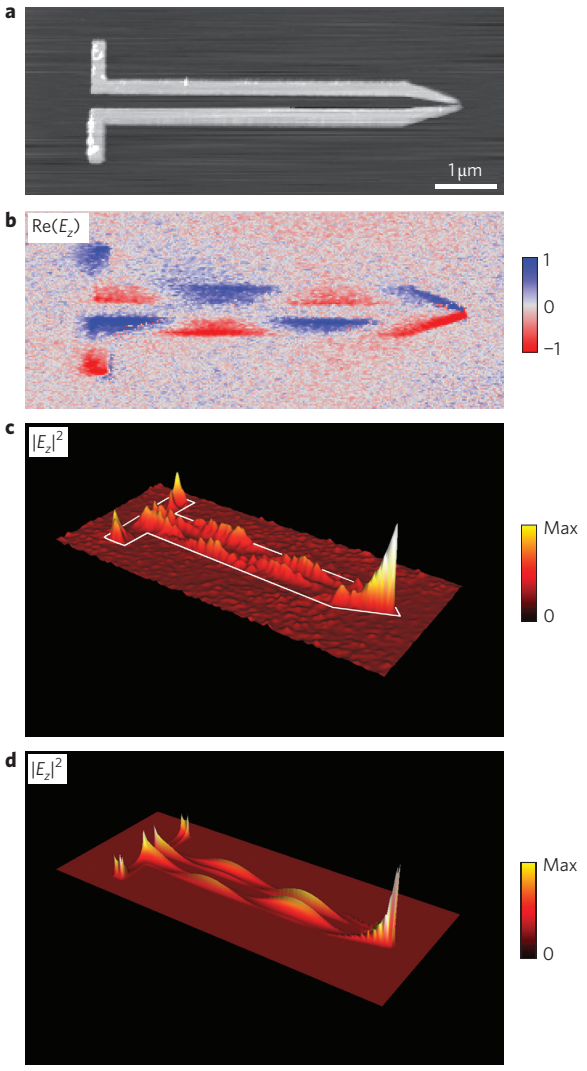

Figure 3 | Nanofocusing of infrared energy with a tapered two-wire transmission line. a, Topography image of the transmission line. **b**, Experimental near-field image showing $\mathrm{Re}(E_z) = |E_z|\cos(\varphi_z)$. Saturated colour scale. **c**, Experimental near-field image showing the intensity of the vertical field component $|E_z|^2$. **d**, Numerically calculated near-field image showing the intensity of the vertical field component $|E_z|^2$.

wire and gap widths (w and g) are reduced, following cases A–C. With decreasing W, both the wavelength and propagation length decrease, which can be attributed to the increasing amount of energy propagating inside the metal (skin depth effect)[28]. Interestingly, even for extremely small W (lines B and C), the propagation length is still of the order of one wavelength λ_{eff}. This indicates the potential to compress the mid-infrared mode by propagating it along a tapered transmission line. Note that the extreme confinement of the surface mode in case C ($W = \lambda/100$) is not accompanied by a strong reduction in the effective wavelength λ_{eff} (Fig. 2f). This finding differs from plasmon compression in tapered metal nanowires at visible frequencies, where the energy accumulation and field enhancement are associated with a significant reduction in the plasmon wavelength[17].

In Fig. 3, we demonstrate experimentally our concept of mid-infrared nanofocusing with a tapered transmission line. Over a length of 1 μm, the total width W of the transmission line (Fig. 3a) is reduced from 700 nm (mode profile A in Fig. 2e) to 90 nm (mode profile C in Fig. 2e). We visualized the propagating mode by imaging the vertical near-field component, analogously to Fig. 2b. It is clearly seen that the field distribution on the transmission lines narrows with decreasing width W, while the asymmetric mode structure (opposite charges on the two wires) is fully retained (Fig. 3b). Remarkably, even close to the taper apex, no fields are observed outside the line, providing experimental evidence of strong field confinement and the absence of leakage fields. To visualize the energy compression, we show in Fig. 3c the intensity of the vertical near-field component $|E_z|^2$. A continuous intensity enhancement can be observed along the taper, as well as intensity modulations along the parallel wires. We attribute the latter to back reflections[32] from the tapered part of the transmission line, in analogy to a non-terminated transmission line at radiofrequencies. At the taper apex, at a distance $x = 6$ μm from the dipole antenna, two extremely confined peaks are observed. The intensity at the peak position is significantly enhanced by a factor of 30 when compared to the intensity measured at $x = 6$ μm on the untapered line (Fig. 2b). Our near-field images were confirmed by a numerical simulation (Fig. 3d) assuming a 5.3-μm-long transmission line, providing the first experimental evidence that mid-infrared energy can be compressed along a tapered transmission line.

To study the vectorial field distribution of the mid-infrared nanofocus, we recorded high-resolution images of both the vertical and horizontal near-field components of the taper region (Fig. 4a). The image of the vertical (out-of-plane) near-field component $|E_z|^2$ reveals two intensity maxima (bright spots) at the taper apex. These maxima appear exactly at the wire tips, as we prove by the superposition of the topography and near-field image (Fig. 4b). The existence of two maxima can be explained by the mode profile (Fig. 2e), showing that the vertical near-field component essentially appears on top of the metal wires. Note that the difference in the peak intensities can be assigned to the slight asymmetric shape of the taper apex. Mapping the horizontal (in-plane) near-field component $|E_y|^2$, we find a single intensity peak inside the gap, located at the taper apex, as predicted by numerical calculations

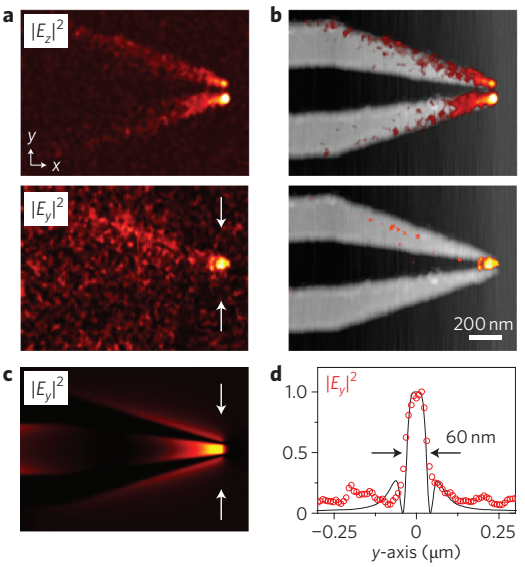

Figure 4 | Vectorial field distribution of the nanofocus. a, High-resolution experimental near-field images of the taper apex, showing the intensity of the vertical and transverse near-field components, $|E_z|^2$ and $|E_y|^2$. **b**, Superposition of near-field intensity and topography. **c**, Numerically calculated near-field image showing the intensity of the horizontal field component, $|E_y|^2$. **d**, Line profile through the nanofocus at the taper apex, showing experimental data (red circles) and calculated data (black line) extracted at the position indicated by the white arrows in **a** and **c**, respectively.

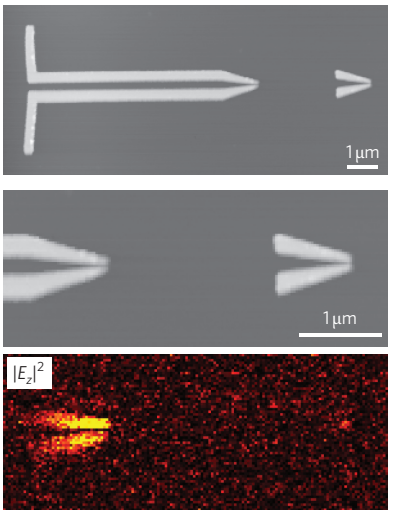

Figure 5 | Control experiment comparing a tapered transmission line with an isolated taper. a, s-SNOM topography image. **b**, Topography and near-field image ($\lambda = 11.2$ μm) showing the intensity of the vertical field component $|E_z|^2$.

(Fig. 4c). From the line profile across the peak (Fig. 4d, extracted at the position indicated by the white arrows in Fig. 4a), we measure an intriguingly small spot size with a diameter of ~60 nm ($\lambda/150$). The high-resolution near-field images provide the first direct experimental evidence that mid-infrared energy can be nanofocused using tapered transmission lines. Remarkably, mid-infrared energy can be nanofocused to a spot size comparable to what has been achieved by plasmon compression in the visible range.

Note that in this experiment the entire transmission-line structure is illuminated. To exclude the possibility that the near-field focus at the taper apex is generated by a local antenna or lightning-rod effect, we compared the tapered transmission line with an isolated taper (Fig. 5). This experiment clearly shows that the isolated taper (Fig. 5b, right) does not generate strong fields at the taper apex. It is only when a propagating transmission-line mode is fed into the taper (Fig. 5b, left) that strong fields are observed at the taper apex.

Nanofocusing of mid-infrared energy with transmission lines opens new avenues for nanoscale imaging and sensing. It enables the development of integrated mid-infrared circuits and devices based on energy transport mediated by surface waves, which will be critical in future infrared-spectroscopic lap-on-a-chip applications, for example. We also stress that both gap and metal wire widths are tapered, providing an infrared nanofocus at a sharply pointed transmission-line apex. Such a structure could be realized on scanning probe tips, allowing for simultaneous high-resolution imaging of sample topography and infrared properties. Furthermore, the near-field images demonstrate the potential of our imaging technique (vector-field nanoscopy[4]) to verify novel fundamental predictions and technological concepts in nanophotonics, plasmonics and metamaterials research. Offering wavelength-independent resolution, it can be used at visible, infrared and terahertz frequencies.

Methods

Sample fabrication. The antennas were fabricated by high-resolution electron-beam lithography and metal lift-off on double-side-polished silicon substrates. A bilayer polymethyl methacrylate (with a molecular weight of 495,000 at the bottom and 950,000 at the top) was used as electron-sensitive polymer. A 40 nm gold film was thermally evaporated in high vacuum on top of a 3-nm-thick titanium layer, electron-beam evaporated for adhesion purposes.

The transmission line shown in Fig. 2 consists of two gold wires (width, 200 nm; length, 15 μm) separated by a 300 nm air gap. The length of the attached dipole antenna was 2 μm. The tapered transmission line shown in Fig. 4 consisted of two gold wires (width, 200 nm; length, 6 μm) separated by a 300 nm air gap. The tapered part of the transmission line measured 1 μm in length, with the widths of the gold wire and gap simultaneously reducing in a linear manner to 20 nm and 50 nm, respectively.

Near-field microscopy set-up. The scattering-type SNOM used for this work is based on an atomic force microscope (AFM). Conventional silicon tips acted as scattering near-field probes. The sample and tip were illuminated from below with a weakly focused CO_2 laser beam (transmission-mode s-SNOM)[9]. Note that the entire transmission line was illuminated. The polarization of the illuminating beam in the presented experiments was parallel to the dipole antenna attached to the transmission line. The near fields scattered by the silicon tip were collected with a parabolic mirror and recorded simultaneously with the sample topography. Background contributions could be fully suppressed by vertical tip oscillation at a frequency $\Omega = 300$ kHz (tapping-mode AFM) and by subsequent higher harmonic demodulation of the detector signal at 3Ω. The amplitude and phase of the in- and out-of-plane near-field components ($|E_y|$ and φ_y, respectively $|E_z|$ and φ_z) were measured with a pseudoheterodyne detection module (www.neaspec.com). The in- and out-of-plane near-field components were obtained by selecting the *s*- and *p*-polarized components of the tip-scattered light with infrared polarizers (www.lasnix.com)[4].

Numerical calculations. The near-field maps of the transmission lines shown in Figs 2c, 3d and 4c were calculated numerically using a commercial finite-difference time-domain (FDTD) software package (Lumerical FDTD solutions, www.lumerical.com). The transmission-line modes shown in Fig. 2e were calculated with an finite-difference frequency-domain (FDFD) mode solver program (Lumerical MODE solutions, www.lumerical.com). For all calculations we assumed a free-space wavelength of 9.3 μm and used the dielectric values for gold from Palik ($\varepsilon_{Au} = -2{,}591 + 1{,}145i$). Good agreement with the experiment data (Figs 2b and 3b) was found when we assumed a refractive index for the silicon substrate of $n_{Si} = 3.07$. We explain this deviation from the tabulated value ($n_{Si,Palik} = 3.44$ at a wavelength of 9.3 μm) by the presence of the titanium adhesion layer, the natural SiO_2 layer on the silicon substrate and by uncertainties in the fabrication process.

Received 3 November 2010; accepted 15 February 2011; published online 4 April 2011

References

1. Gutberlet, A. *et al.* Aggregation-induced dissociation of $HCl(H_2O)_4$ below 1 K: the smallest droplet of acid. *Science* **324,** 1545–1548 (2009).
2. Li, Z. Q. *et al.* Dirac charge dynamics in graphene by infrared spectroscopy. *Nature Phys.* **4,** 532–535 (2008).
3. Soref, R. Mid-infrared photonics in silicon and germanium. *Nature Photon.* **4,** 495–497 (2010).
4. Schnell, M., Garcia-Etxarri, A., Alkorta, J., Aizpurua, J. & Hillenbrand, R. Phase-resolved mapping of the near-field vector and polarization state in nanoscale antenna gaps. *Nano Lett.* **10,** 3524–3528 (2010).
5. Olmon, R. L. *et al.* Determination of electric-field, magnetic-field, and electric-current distributions of infrared optical antennas: a near-field optical vector network analyzer. *Phys. Rev. Lett.* **105,** 167403 (2010).
6. Mühlschlegel, P., Eisler, H.-J., Martin, O. J. F., Hecht, B. & Pohl, D. W. Resonant optical antennas. *Science* **308,** 1607–1609 (2005).
7. Taminiau, T. H., Stefani, F. D., Segerink, F. B. & Van Hulst, N. F. Optical antennas direct single-molecule emission. *Nature Photon.* **2,** 234–237 (2008).
8. Bharadwaj, P., Deutsch, B. & Novotny, L. Optical antennas. *Adv. Opt. Photon.* **1,** 438–483 (2009).
9. Schnell, M. *et al.* Controlling the near-field oscillations of loaded plasmonic nanoantennas. *Nature Photon.* **3,** 287–291 (2009).
10. Schuller, J. A. *et al.* Plasmonics for extreme light concentration and manipulation. *Nature. Mater.* **9,** 193–204 (2010).
11. Xu, H., Bjerneld, E. J., Käll, M. & Börjesson, L. Spectroscopy of single hemoglobin molecules by surface enhanced Raman scattering. *Phys. Rev. Lett.* **83,** 4357–4360 (1999).
12. Soukoulis, C. M., Linden, S. & Wegener, M. Negative refractive index at optical wavelengths. *Science* **315,** 47–49 (2007).
13. Engheta, N. Circuits with light at nanoscales: optical nanocircuits inspired by metamaterials. *Science* **317,** 1698–1702 (2007).
14. Xu, H., Aizpurua, J., Käll, M. & Apell, P. Electromagnetic contributions to single-molecule sensitivity in surface-enhanced Raman scattering. *Phys. Rev. E* **62,** 4318–4324 (2000).
15. Novotny, L. & Hafner, C. Light propagation in a cylindrical waveguide with a complex, metallic, dielectric function. *Phys. Rev. E* **50,** 4094–4106 (1994).
16. Keilmann, F. Surface-polariton propagation for scanning near-field optical microscopy application. *J. Microsc.* **194,** 567–570 (1999).
17. Stockman, M. I. Nanofocusing of optical energy in tapered plasmonic waveguides. *Phys. Rev. Lett.* **93,** 137404 (2004).

18. Verhagen, E., Spasenovicacute, M., Polman, A. & Kuipers, L. Nanowire plasmon excitation by adiabatic mode transformation. *Phys. Rev. Lett.* **102,** 203904 (2009).
19. De Angelis, F. *et al.* Nanoscale chemical mapping using three-dimensional adiabatic compression of surface plasmon polaritons. *Nature Nanotech.* **5,** 67–72 (2010).
20. Ropers, C. *et al.* Grating-coupling of surface plasmons onto metallic tips: a nanoconfined light source. *Nano Lett.* **7,** 2784–2788 (2007).
21. Pile, D. F. P. & Gramotnev, D. K. Adiabatic and nonadiabatic nanofocusing of plasmons by tapered gap plasmon waveguides. *Appl. Phys. Lett.* **89,** 041111 (2006).
22. Choi, H., Pile, D. F., Nam, S., Bartal, G. & Zhang, X. Compressing surface plasmons for nano-scale optical focusing. *Opt. Express* **17,** 7519–7524 (2009).
23. Vedantam, S. *et al.* A plasmonic dimple lens for nanoscale focusing of light. *Nano Lett.* **9,** 3447–3452 (2009).
24. Neacsu, C. C. *et al.* Near-field localization in plasmonic superfocusing: a nanoemitter on a tip. *Nano Lett.* **10,** 592–596 (2010).
25. Wang, K. & Mittleman, D. M. Metal wires for terahertz wave guiding. *Nature* **432,** 376–379 (2004).
26. Pendry, J. B., Martin-Moreno, L. & Garcia-Vidal, F. J. Mimicking surface plasmons with structured surfaces. *Science* **305,** 847–848 (2004).
27. Maier, S. A., Andrews, S. R., Martin-Moreno, L. & Garcia-Vidal, F. J. Terahertz surface plasmon-polariton propagation and focusing on periodically corrugated metal wires. *Phys. Rev. Lett.* **97,** 176805 (2006).
28. Rusina, A., Durach, M., Nelson, K. A. & Stockman, M. I. Nanoconcentration of terahertz radiation in plasmonic waveguides. *Opt. Express* **16,** 18576–18589 (2008).
29. Akalin, T., Treizebre, A. & Bocquet, B. Single-wire transmission lines at terahertz frequencies. *IEEE Trans. Microw. Theory* **54,** 2762–2767 (2006).
30. Zhan, H., Mendis, R. & Mittleman, D. M. Superfocusing terahertz waves below λ/250 using plasmonic parallel-plate waveguides. *Opt. Express* **18,** 9643–9650 (2010).
31. Mandviwala, T., Lail, B. & Boreman, G. Infrared-frequency coplanar striplines: design, fabrication, and measurements. *Microw. Opt. Technol. Lett.* **47,** 17–20 (2005).
32. Krenz, P. M., Olmon, R. L., Lail, B. A., Raschke, M. B. & Boreman, G. D. Near-field measurement of infrared coplanar strip transmission line attenuation and propagation constants. *Opt. Express* **18,** 21678–21686 (2010).
33. Huang, J.-S., Feichtner, T., Biagioni, P. & Hecht, B. Impedance matching and emission properties of nanoantennas in an optical nanocircuit. *Nano Lett.* **9,** 1897–1902 (2009).

Acknowledgements

This work was supported by European FP7 project 'Nanoantenna' (FP7-HEALTH-F5-2009-241818-NANOANTENNA) and National Projects MAT2009-08393 and MAT2009-08494 from the Spanish Ministerio de Ciencia e Innovacion. M.S. and L.A. acknowledge financial support from the 'Programa de Formación de Personal Investigador' promoted by the Department of Education, Universities and Research of the Basque Government. P.A.-G. acknowledges technical support from A.A. González.

Author contributions

M.S. and R.H. conceived the experiments. P.A.-G., F.C., L.A., L.E.H. and A.C. contributed to sample preparation. M.S. and P.A.-G. performed the experiments. M.S. carried out the calculations. M.S. and R.H. analysed the data and wrote the manuscript.

Additional information

The authors declare no competing financial interests. Reprints and permission information is available online at http://www.nature.com/reprints/. Correspondence and requests for materials should be addressed to R.H.